Available online at www.sciencedirect.com
SCIENCE DIRECT
International Journal of Heat and Mass Transfer 49 (2006) 1937–1945
International Journal of HEAT and MASS TRANSFER
www.elsevier.com/locate/ijhmt

Heat and mass transfer for liquid film evaporation along a vertical plate covered with a thin porous layer

Jin-Sheng Leu [a], Jiin-Yuh Jang [b,*], Yin Chou [b]

[a] Department of Mechanical Engineering, Air Force Institute of Technology, Kaohsiung 82042, Taiwan
[b] Department of Mechanical Engineering, National Cheng-Kung University, Tainan 70101, Taiwan

Received 7 June 2005; received in revised form 8 November 2005
Available online 10 January 2006

Abstract

The purpose of this work is to evaluate the heat and mass enhancement of liquid film evaporation by covering a porous layer on the plate. Liquid and gas streams are approached by two coupled laminar boundary layers incorporated with non-Darcian modes. The numerical solution is obtained by utilizing a fully implicit finite difference method and examined in detail for the effects of porosity ε, porous layer thickness δ, ambient relative humidity ϕ and Lewis number Le on the average heat and mass transfer performance. It is shown that the heat and mass transfer performance may be enhanced by the presence of a porous layer. Both the average Nusselt and Sherwood numbers are increased with the decrease of ε, δ and ϕ. In addition, the influence of ε on the heat and mass transfer is significantly increased as δ is increased.

Keywords: Liquid film evaporation; Porous medium; Heat and mass transfer

1. Introduction

Liquid film evaporation is one effective latent heat transfer mechanism widely utilized in industrial fields such as chemical distillation, air conditioning, cooling towers, drying, and desalination. The physical scheme consists of a thin liquid film flowing down along a heated plate, with the liquid film exposed to a forced gas stream. Because part of the liquid evaporates into the gas stream, liquid film evaporation possesses a high heat transfer coefficient, low feed rates and other inherent advantages. However, the theoretical analysis of liquid film evaporation problem is inherently complicated because the transport phenomena involve the coupled heat and mass transfer at the liquid film–gas interface.

Previous research usually examined the problem based on simplified 1-D and 2-D mathematical models. The 1-D model was used to develop the governing conservation of mass, mass species, momentum and energy by the conservation laws to the control volumes of the liquid film and moist air [1–4]. MaClaine-Cross and Bank [1,2] analyzed the heat and mass transfer characteristics in a wet surface heat exchanger. Their results are 20% higher than the experimental data. Wassel and Mills [3] illustrated a 1-D design methodology for a counter-current falling film evaporative cooler. The narrow flow passages were found to be more effective than conventional designs for the thermal performance of the evaporative condenser. A 1-D model of heat and mass transfer in the evaporative cooling process that takes place in a single-tube exchanger was formulated by Perez-Blanco and Bird [4]. The early 2-D model literature focused on heat and mass transfer in the gas stream, with the liquid film supposed to be at rest and with a very thin constant thickness. The vaporizing liquid film is treated as the boundary condition for the gas stream [5,6] and the temperature distributions across the film are assumed to be linear [7,8].

* Corresponding author. Tel.: +886 6 2088573/2757575x62148; fax: +886 6 2753850.
E-mail address: jangjim@mail.ncku.edu.tw (J.-Y. Jang).

0017-9310/$ - see front matter © 2005 Elsevier Ltd. All rights reserved.
doi:10.1016/j.ijheatmasstransfer.2005.11.004

Nomenclature

d	thickness of porous layer (m)
d_p	particle diameter (m)
D	mass diffusivity ($m^2\ s^{-1}$)
Da	Darcy number, $Da = K/d^2$
Fr	Froude number, $Fr = U_{g,\infty}/\sqrt{gL}$
g	gravitational acceleration ($m\ s^{-2}$)
$h_{t,x}$	local heat transfer coefficient ($W\ m^{-2}\ °C^{-1}$)
$h_{m,x}$	local mass transfer coefficient ($W\ m^{-2}\ °C^{-1}$)
h_{fg}	latent heat of vaporization ($J\ kg^{-1}$)
K	permeability of the porous layer (m^2)
k	thermal conductivity, ($W\ m^{-1}\ °C^{-1}$)
L	plate length (m)
Le	Lewis number, $Le = \alpha/D$
M	molar mass ($kg\ mol^{-1}$)
m''_v	vapor mass flux ($kg\ m^{-2}\ s^{-1}$)
Nu	average Nusselt number
P	pressure (Pa)
Pr	Prandtl number
q''_l	latent heat flux ($W\ m^{-2}$)
q''_s	sensible heat flux ($W\ m^{-2}$)
Re_g	gas Reynolds number, $Re_g = u_{g,\infty}L/\nu_g$
Sh	average Sherwood number
T	temperature (°C)
U, V	dimensionless velocity
u, v	velocity along x, y coordinates ($m\ s^{-1}$)
X, Y	dimensionless coordinates
x, y	coordinate (m)

Greek symbols

α	effective thermal diffusivity ($m^2\ s^{-1}$)
δ	dimensionless thickness of porous layer
ε	porosity
θ	dimensionless temperature, $\theta = (T - T_{g,\infty})/(T_w - T_{g,\infty})$
Γ	dimensionless inertia coefficient of porous medium, $\Gamma = Cu_l\sqrt{K}/\nu_l$
λ	dimensionless concentration, $\lambda = (\omega - \omega_\infty)/(\omega_w - \omega_\infty)$
τ	shear stress (Pa)
μ	dynamic viscosity ($kg\ s^{-1}\ m^{-1}$)
ν^*	kinematic viscosity ratio of liquid to gas, $\nu^* = \nu_l/\nu_g$
ρ	mass density ($kg\ m^{-3}$)
ϕ	relative humidity at inlet
ω	vapor mass concentration (ρ_v/ρ_g)

Subscripts

g	gas stream (air + vapor)
i	liquid–gas interface
l	liquid film
v	vapor
w	wall
∞	inlet or free stream condition

Recently, researches with more rigorous treatments of the equations governing the liquid film and liquid–gas interface have been published. Yan and Lin [9] studied the evaporative cooling of liquid film through interfacial heat and mass transfer in a vertical channel. Yan and Soong [10] presented their numerical solution for convective heat and mass transfer along an inclined heated plate with film evaporation. Tsay [11] numerically analyzed the cooling characteristics of a wet surface heat exchanger with a liquid film evaporating into a countercurrent moist air flow. The studies above [9–11] neglected inertia in the momentum equation and the normal convection term in the heat equation for liquid film flow, thus the liquid film flow is simplified to a 1-D momentum equation and 1-D (or 2-D) heat equation. The complete two-dimensional boundary layer model for the evaporating liquid and gas flows along an inclined plate was studied recently by Mezaache and Daguenet [12]. Their parametric study focused on the effects of inlet conditions such as gas velocity, liquid mass flow rate and inclined angles and their interaction with both isothermal and heated walls. The results indicate that a larger liquid mass flow rate and smaller gas velocity cause an enhancement of the inclination effect on the heat and mass transfer.

The preceding literature review shows that most of the theoretical research into evaporating liquid film flow focused on the coupled heat and mass transfer characteristics for various inlet and geometrical conditions. In addition, all these analyses were restricted to the study of the liquid film flow with flat solid surface. Recently, the heat and mass transfer enhancement technique from liquid film evaporation have received considerable attention. One well known method is to roughen the surface either randomly with sand grains, or to add regular geometric roughness elements (rib, rod, etc.) on the surface [13–16]. These studies focused on developing accurate predictions of the behavior of a given roughness geometry and finding the optimum geometry for a given flow friction. Another method is to utilize a porous structure composite for the plate to provide a large contact area and thereby increase the heat and mass transfer [17–21]. For the studies of heat and mass transfer for liquid film flow in porous medium, Rees and Vafai [17] investigated the free convection boundary layer flow of a Darcy–Brinkman fluid induced by a horizontal surface embedded in a fluid-saturated porous layer. The paper was described in detail how boundary friction affects the free convective flow pattern in a porous medium. Haddad et al. [18] investigated the validity of the local thermal equilibrium assumption in the case of free convection flow over an isothermal flat plate embedded in a porous medium. Alazmi and Vafai [19] analyzed in detail the fluid flow and heat

transfer interfacial conditions between a porous medium and a fluid layer. They proposed a set of correlations for interchanging the interface velocity and temperature as well as the average Nusselt number among various models. Zhao [20] studied the coupled heat and mass transfer in a stagnation point flow of air through a heated porous bed with thin liquid film evaporation. To achieve the analytical solution, the paper assumed the liquid layer was very thin and stationary, and the air stream was idealized as the stagnation point flow pattern. Diky et al. [21] carried out an experiment for liquid film evaporation in heated gas flow in a contact apparatus with a porous packing.

Until now, there seems to be no related theoretical analysis to evaluate the feasibility of utilizing porous materials for the heat transfer enhancement of falling liquid evaporation. Part of the reason is the coupled heat and mass transfer process becomes more complicated in the presence of a porous medium. This has motivated the present investigation. The present study analyzes the liquid film evaporation flow along a vertical isothermal plate covered with a thin liquid-saturated porous layer. A two-dimensional steady laminar boundary layer model is adopted for the gas and liquid streams. The non-Darcian inertia and boundary effects are included to describe the governing equations of the liquid-saturated porous medium. The governing equations are discretized to a fully implicit difference representation and solved by the tridiagonal matrix method. The aim of this work is to evaluate the effect of the porous layer on heat and mass transfer. The corresponding parametric analyses on features such as gas inlet conditions (Reynolds number and ambient relative humidity) and the structural properties of the porous material (porosity and thickness of the porous layer) on the performance of liquid film evaporation are examined in detail.

2. Mathematical analysis

As shown schematically in Fig. 1, the problem concerns a vertical isothermal plate, on which the wall temperature is T_w. A thin porous layer of thickness d is covered on the plate. The plate is wetted by a falling liquid film with an inlet temperature $T_{l,in}$ and inlet flow rate $m_{l,in}$. The liquid film is exposed to a co-current forced gas flow at free stream velocity $u_{g,\infty}$, ambient temperature $T_{g,\infty}$, and mass concentration ω_∞. Heat is transferred from the plate to the liquid film and across to the gas stream. The gas flow is assumed as laminar and steady, with the usual boundary layer approximations. The liquid-saturated porous medium is isotropic and homogeneous, and the local thermal equilibrium assumption is valid in this case. In addition, we assume that the liquid–gas interface is invariantly located at the surface of the porous layer.

(a) Liquid film region

Under the assumption of thin liquid film, the order of magnitude analysis showed that the inertia terms in the momentum equation can be neglected as compared with the diffusion term. Furthermore, the longitudinal gradients

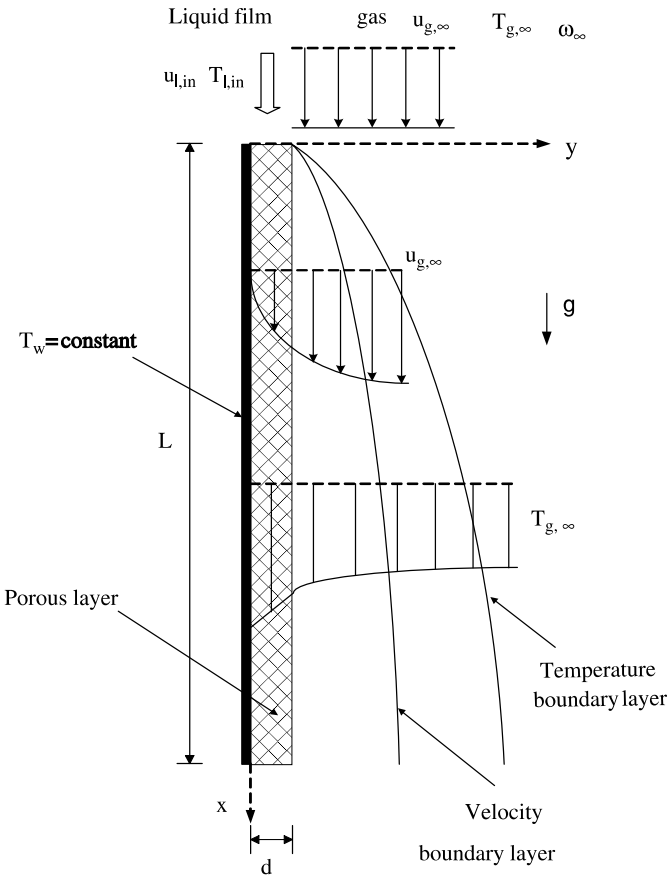

Fig. 1. Schematic diagram of the physical system.

of velocity and temperature are much smaller than those in the transverse direction. By including the non-Darcian models of boundary viscous and inertia effects, the momentum and energy boundary layer equations are as follows:

$$0 = \rho_l g + \frac{\mu_l}{\varepsilon}\frac{\partial^2 u_l}{\partial y^2} - \frac{\mu_l}{K}u_l - \frac{\rho_l C}{\sqrt{K}}u_l^2, \tag{1}$$

$$u_l\frac{\partial T_l}{\partial x} = \alpha_e\frac{\partial^2 T_l}{\partial y^2}, \tag{2}$$

where the subscript "l" represents the variables of the liquid stream. K is the permeability of the porous medium, C is the flow inertia parameter [22], ε is the porosity and α_e is the effective thermal diffusivity.

(b) Gas stream region

The two-dimensional laminar continuity, momentum, energy and concentration equations can be written as

$$\frac{\partial u_g}{\partial x} + \frac{\partial v_g}{\partial y} = 0, \tag{3}$$

$$u_g\frac{\partial u_g}{\partial x} + v_g\frac{\partial u_g}{\partial y} = v_g\frac{\partial^2 u_g}{\partial y^2}, \tag{4}$$

$$u_g\frac{\partial T_g}{\partial x} + v_g\frac{\partial T_g}{\partial y} = \alpha_g\frac{\partial^2 T_g}{\partial y^2}, \tag{5}$$

$$u_g\frac{\partial \omega}{\partial x} + v_g\frac{\partial \omega}{\partial y} = D\frac{\partial^2 \omega}{\partial y^2}, \tag{6}$$

where the subscript "g" represents the variables of the gas stream. ω, ρ, ν, α and D are the mass concentration, density, kinematic viscosity, thermal diffusivity and mass diffusivity of the gas.

(c) The corresponding boundary and interface matching conditions at inlet ($x = 0$)

$$T_l = T_{l,in}, \quad T_g = T_{g,\infty}, \quad u_g = u_{g,\infty}, \quad \omega = \omega_\infty \tag{7}$$

at wall and free stream ($y = 0, \infty$)

$$\begin{aligned} &\text{at } y = 0, \quad u_l = 0, \ T_l = T_w, \\ &\text{at } y = \infty, \quad u_g = u_{g,\infty}, \ v_g = 0, \ T_g = T_{g,\infty}, \ \omega = \omega_\infty \end{aligned} \tag{8}$$

at interface ($y = d$)

$$u_i = u_{l,i} = u_{g,i}, \quad T_i = T_{l,i} = T_{g,i}, \tag{9}$$

$$v_{g,i} = -\frac{D}{1-\omega_i}\left(\frac{\partial \omega}{\partial y}\right)_i, \tag{10}$$

$$\left(\mu_l \frac{\partial u}{\partial y}\right)_{l,i} = \left(\mu_g \frac{\partial u}{\partial y}\right)_{g,i} = \tau_i, \tag{11}$$

$$q''_t = -k_l\left(\frac{\partial T_l}{\partial y}\right)_i \quad \text{and} \quad q''_t = q''_s + q''_l = -k_g\left(\frac{\partial T_g}{\partial y}\right)_i + m''_v h_{fg}. \tag{12}$$

Eqs. (11) and (12) express the continuity of shear stress and energy balance at the gas–liquid interface. The total heat flux from the wall q''_t can be transferred to two modes: One is the sensible heat flux via gas temperature gradient q''_s, the other is the latent heat flux via the liquid film vaporization q''_l.

During the calculated procedure, the interfacial evaporating mass flux is given by

$$m''_v = \rho_g v_{g,i} = -\frac{\rho_g D}{1-\omega_i}\left(\frac{\partial \omega}{\partial y}\right)_i. \tag{13}$$

And the mass concentration ω_i is expressed as

$$\omega_i = \frac{M_v}{M_g}\frac{p_{v,i}}{p_g}, \tag{14}$$

where $P_{v,i}$ is the partial pressure of the saturated vapor at the gas–liquid interface. The inlet mass flow rate of the liquid film can be evaluated by [23]

$$m_{l,in} = \frac{\rho_l g}{3\nu_l} d^3 \varepsilon^3. \tag{15}$$

The conservation equations can be recast into dimensionless forms by adopting the following dimensionless variables:

$$\begin{aligned} &X = \frac{x}{L}, \quad Y_g = \frac{y}{L}\sqrt{Re_g}, \quad Y_l = \frac{y}{d}, \quad \delta = \frac{d}{L}, \\ &U_g = \frac{u_g}{u_{g,\infty}}, \quad V_g = \frac{v_g}{u_{g,\infty}}, \quad U_l = \frac{u_l}{u_{g,\infty}}, \\ &\theta_g = \frac{T_g - T_{g,\infty}}{T_w - T_{g,\infty}}, \quad \theta_l = \frac{T_l - T_{g,\infty}}{T_w - T_{g,\infty}}, \quad \lambda = \frac{\omega - \omega_\infty}{\omega_w - \omega_\infty}, \end{aligned} \tag{16}$$

where δ is the porous layer thickness ratio to plate length. ω_w is the corresponding mass concentration at the wall temperature T_w. The other symbols are defined in the nomenclature.

The dimensionless governing equation (1)–(6) are

Liquid film region:

$$0 = \frac{Re_g \cdot \delta^2}{\nu^* \cdot Fr^2} + \frac{1}{\varepsilon}\frac{\partial^2 U_l}{\partial Y_l^2} - \frac{1}{Da}\cdot U_l - \frac{\Gamma}{Da}\cdot U_l^2, \tag{17}$$

$$U_l \frac{\partial \theta_l}{\partial X} = \frac{\nu^*}{\delta^2 Pr_e Re_g}\frac{\partial^2 \theta_l}{\partial Y_l^2}; \tag{18}$$

Gas stream region:

$$\frac{\partial U_g}{\partial X} + \sqrt{Re_g}\frac{\partial V_g}{\partial Y_g} = 0, \tag{19}$$

$$U_g \frac{\partial U_g}{\partial X} + \sqrt{Re_g} V_g \frac{\partial U_g}{\partial Y_g} = \frac{\partial^2 U_g}{\partial Y_g^2}, \tag{20}$$

$$U_g \frac{\partial \theta_g}{\partial X} + V_a\sqrt{Re_g}\frac{\partial \theta_g}{\partial Y_g} = \frac{1}{Pr_g}\frac{\partial^2 \theta_g}{\partial Y_g^2}, \tag{21}$$

$$U_g \frac{\partial \lambda}{\partial X} + V_g\sqrt{Re_g}\frac{\partial \lambda}{\partial Y_g} = \frac{1}{Pr_g Le}\frac{\partial^2 \lambda}{\partial Y_g^2}; \tag{22}$$

where $\nu^* = \nu_l/\nu_g$ is the kinematic viscosity ratio of liquid to gas, $Da = K/d_p^2$ is the Darcy number of the porous medium, $\Gamma = Cu_l\sqrt{K}/\nu_l$ is the dimensionless inertia coefficient of non-Darcy flow. The dimensionless groups such as Re_g (gas Reynolds number), Pr (Prandtl number), Le (Lewis number) and Fr (Froude number) are defined as

$$\begin{aligned} &Re_g = \frac{\rho_g u_{g,\infty} L}{\mu_g}, \quad Le = \frac{\alpha_g}{D}, \quad Fr = \frac{u_{g,\infty}}{\sqrt{gL}}, \\ &Pr_g = \frac{\nu_g}{\alpha_g}, \quad Pr_e = \frac{\nu_l}{\alpha_e}. \end{aligned} \tag{23}$$

The corresponding dimensionless boundary conditions are as follows:

at inlet ($X = 0$):

$$\theta_l = \theta_{l,in}, \quad \theta_g = 0, \quad U_g = 1, \quad \lambda = 0; \tag{24}$$

at wall and free stream ($Y_l = 0$, $Y_g = \infty$):

$$\begin{aligned} &\text{at } Y_l = 0, \quad U_l = 0, \ \theta_l = 1, \\ &\text{at } Y_g = \infty, \quad U_g = 1, \ V_g = 0, \ \theta_g = 0, \ \lambda = 0; \end{aligned} \tag{25}$$

at interface ($Y_l = 1$):

$$U_i = U_{l,i} = U_{g,i}, \quad \theta_i = \theta_{l,i} = \theta_{g,i}, \tag{26}$$

$$V_{g,i} = -\frac{(\omega_{w,in} - \omega_\infty)}{(1-\omega_i)}\frac{1}{Pr_g Le\sqrt{Re_g}}\left(\frac{\partial \lambda}{\partial Y_g}\right)_i \tag{27}$$

$$\left(\frac{\partial U_l}{\partial Y_l}\right)_i = \sqrt{Re_g}\left(\frac{\rho_g}{\rho_l}\right)\frac{1}{\nu^*}\delta\left(\frac{\partial U_g}{\partial Y_g}\right)_i, \tag{28}$$

$$\left(\frac{\partial \theta_l}{\partial \eta_l}\right)_i = \sqrt{Re_g}\frac{k_a}{k_e}\delta\left(\frac{\partial \theta_g}{\partial \eta_g}\right)_i + \sqrt{Re_g}\frac{\rho_g D h_{fg}(\omega_{w,in} - \omega_\infty)}{k_e(1-\omega_i)(T_w - T_\infty)}\delta\left(\frac{\partial \lambda}{\partial Y_g}\right)_i. \tag{29}$$

The local heat transfer coefficient $h_{t,x}$ at the interface is defined as

$$h_{t,x} = \frac{q''_t}{(T_w - T_{g,\infty})} = \frac{\left(-k_g \frac{\partial T}{\partial y}\right)_i}{(T_w - T_{g,\infty})} + \frac{m''_v \cdot h_{fg}}{(T_w - T_{g,\infty})}. \quad (30)$$

It should be noted that the reference temperature difference used in Eq. (30) is defined as $(T_w - T_{g,\infty})$ instead of $(T_i - T_{g,\infty})$. This is because $(T_i - T_{g,\infty})$ is an unknown and changeable value, and is not applicable for non-dimensionalized analysis. The average Nusselt number over the length L of the plate is written as

$$Nu = \frac{\int_0^L h_{t,x}\,dx}{k_g}. \quad (31)$$

Incorporating with Eq. (13), the local mass transfer coefficient $h_{m,x}$ is defined as

$$h_{m,x} = \frac{m''_{v,i}(1-\omega_i)}{\rho_g(\omega_w - \omega_\infty)}. \quad (32)$$

The average Sherwood number over the length L of the plate is written as

$$Sh = \frac{\int_0^L h_{m,x}\,dx}{D}. \quad (33)$$

3. Numerical method

The coupled governing equations (17)–(22) are parabolic at X, thus the finite difference solutions for these equations can be marched along the downstream direction at the beginning $X = 0$. The governing equations are discretized to a fully implicit difference representation, in which the upwind scheme is used to model the axial convective terms, while second-order central difference schemes are employed for the transverse convection and diffusion terms. Newton linearization procedure is used to linearize the nonlinear terms of Eqs. (17)–(22). The resulting discretization equations can be written in "block-tridiagonal" form and solved by the tridiagonal matrix method. The solving procedure is similar to that described in detail by Mezaache and Daguenet [12]. The grid system of $I \times J \times K = 101 \times 81 \times 51$ grid points is adopted typically in the computation domain (I: total grid points along the plate, J: total grid points across the gas boundary and K: total grid points across the liquid film) and the divergence-free criterion is 10^{-5}. A careful check for the grid-independence of the numerical solutions has been made to ensure the accuracy and validity of the numerical results. For this purpose, five grid systems $201 \times 101 \times 65$, $101 \times 101 \times 65$, $101 \times 81 \times 51$, $101 \times 41 \times 46$ and $51 \times 41 \times 46$ were tested for specific case of $Re_g = 50{,}000$, $\varepsilon = 0.4$, $\delta = 0.01$, and $\phi = 70\%$. The comparisons of the average Nusselt and Sherwood numbers for the tested grid systems and their errors relative to the grid system $201 \times 101 \times 65$ are tabulated in Table 1.

Table 1
Comparisons of average Nu and Sh numbers for five grid systems at $Re_g = 50{,}000$, $\varepsilon = 0.4$, $\delta = 0.01$ and $\phi = 70\%$

Grid systems	Nu		Sh	
	Value	Relative error (%)	Value	Relative error (%)
$201 \times 101 \times 66$	401.40	–	24.14	–
$101 \times 101 \times 66$	404.64	0.8	24.36	0.91
$101 \times 81 \times 51$	405.15	0.93	24.37	0.95
$101 \times 41 \times 46$	385.37	4.00	23.17	4.02
$51 \times 41 \times 46$	395.15	1.56	23.79	1.45

4. Results and discussion

The present study mainly evaluates the influence of utilizing porous material on the heat and mass transfer performance of evaporating liquid film flow. Emphasis is placed on the coupled effects of the porosity ε, thickness of porous layer δ on the local transport phenomena and average heat and mass transfer performances with gas Reynolds number Re_g ranging from 10^4 to 10^5 ($u_{g,\infty} = 0.15$–1.5 m/s). In respect to practical situations, certain conditions are selected: $P_\infty = 1$ atm, $T_w = 60$ °C, $T_{l,in} = T_{g,\infty} = 27$ °C, $L = 0.5$ m. The liquid and gas are water and humid air, respectively.

Fig. 2 presents the axial distribution of dimensionless liquid–gas interfacial temperature θ_i for selected values of Re_g ($Re_g = 10{,}000$, $50{,}000$) and ε ($\varepsilon = 0.4$, 0.8, 1.0) at $\delta = 0.01$ and $\phi = 70\%$. It is noted that the results for $\varepsilon = 1$ correspond to the case of liquid film flow without a porous layer, and are achieved at $\Gamma = 0$, $Da \to \infty$. Fig. 2 shows that θ_i increases dramatically with the axial location X in the beginning and smoothes down gradually after $X = 0.25$. Additionally, it is found that lower θ_i is noted

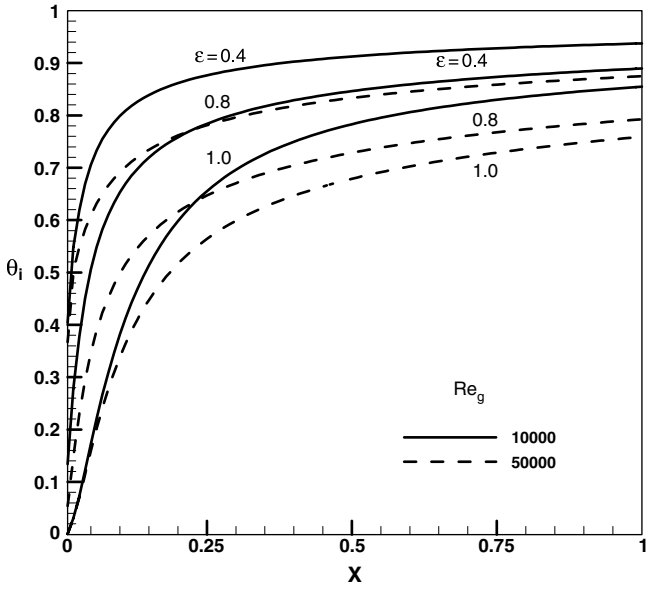

Fig. 2. Axial distribution of dimensionless interfacial temperature for various Re_g and ε with $\delta = 0.01$ and $\phi = 70\%$.

with a higher Re_g. This confirms the general concept that the heat and mass transfer is more effective for a higher Reynolds flow. Fig. 2 also shows that a higher interfacial temperature is found for lower porosity ε. It means that a liquid-saturated porous layer can increase the liquid–gas interfacial temperature. The reason is the porous layer increases the heat transfer area of the liquid film and lets heat more effectively transfer to the liquid film.

The corresponding axial distributions of dimensionless mass concentration λ_i and liquid evaporating rate m''_v are presented in Figs. 3 and 4, respectively. The axial distributions of λ_i follow the same trend as the θ_i shown in Fig. 3, due to a higher interfacial temperature which results in a higher mass concentration. In addition, similar results are achieved so that λ_i is higher for lower ε and Re_g. When comparing Figs. 2 and 3, the effects of ε and Re_g on the mass concentration seem more significant than those on the temperature profiles. Fig. 4 shows the axial distribution of liquid evaporation rate m''_v with various ε and Re_g. For lower ε and higher Re_g, greater liquid film vaporization is observed, due to the fact that a higher interfacial temperature causes a higher mass concentration, which then results in a larger concentration gradient at the interface.

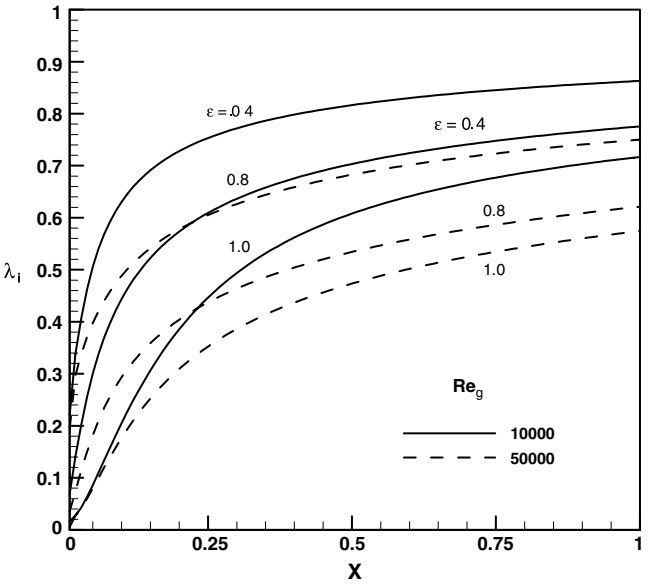

Fig. 3. Axial distribution of dimensionless interfacial mass concentration for various Re_g and ε with $\delta = 0.01$ and $\phi = 70\%$.

As is well known, latent heat flux is the dominant mode of heat transfer in liquid film evaporation. Thus, it is essential to evaluate the influence of porous structures on the sensible and latent heat transfers. The axial distributions of the latent and sensible heat transfer rates (q''_l/q''_t and q''_s/q''_t) for various ε ($\varepsilon = 0.4$, 0.8, 1.0) at $Re_g = 10{,}000$, $\delta = 0.01$ and $\phi = 70\%$ are presented in Fig. 5. It shows that the latent heat transfer is about ten times larger than the sensible heat transfer. It is also seen that a lower ε results in a higher q''_l/q''_t and a lower q''_s/q''_t. Thus, a lower porosity porous layer tends to increase the importance of the role of latent heat transfer.

Fig. 6(a) and (b) present the variations of the average Nusselt (Nu) and Sherwood (Sh) numbers, respectively, with Re_g for specific values of ε ($\varepsilon = 0.4$, 0.8, 1.0) at $\delta = 0.01$ and $\phi = 70\%$. It is seen that, as would be expected, the Nu and Sh increase with the increase of Re_g. In addition, larger Nu and Sh are obtained for lower ε. And the influence of ε on the Nu and Sh is more significant at the larger Re_g. For the case of $Re_g = 100{,}000$, Nu and Sh for $\varepsilon = 0.4$ are increased by about 24% and 30% relative to the value for $\varepsilon = 1.0$ (without porous medium).

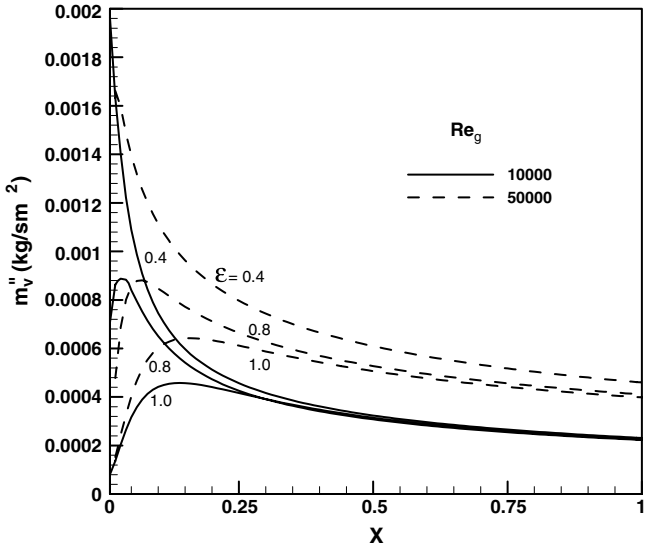

Fig. 4. Evaporating flux of liquid at every axial location for various Re_g and ε with $\delta = 0.01$ and $\phi = 70\%$.

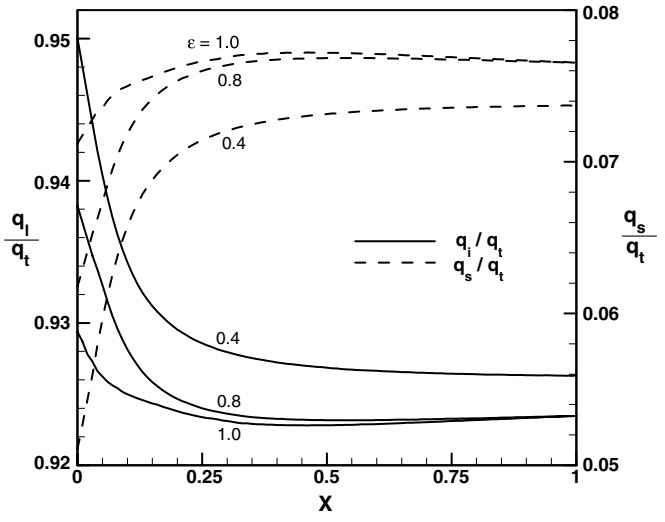

Fig. 5. Axial distribution of latent heat flux q_l/q_t and sensible heat flux q_s/q_t for various ε with $Re_g = 10{,}000$, $\delta = 0.01$ and $\phi = 70\%$.

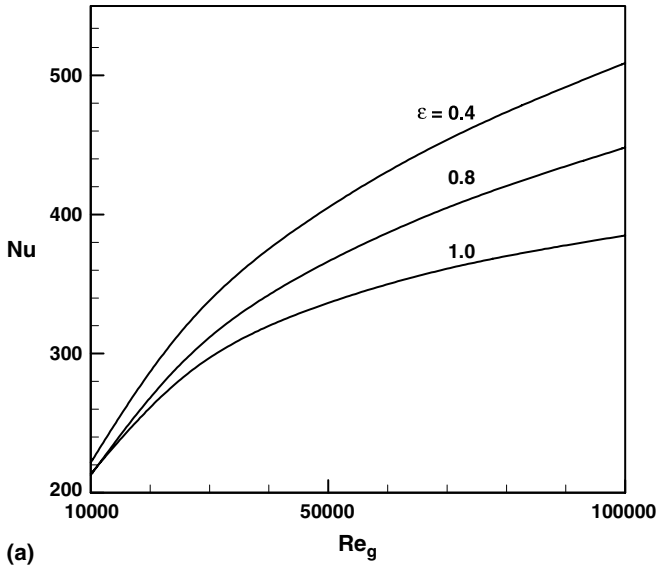

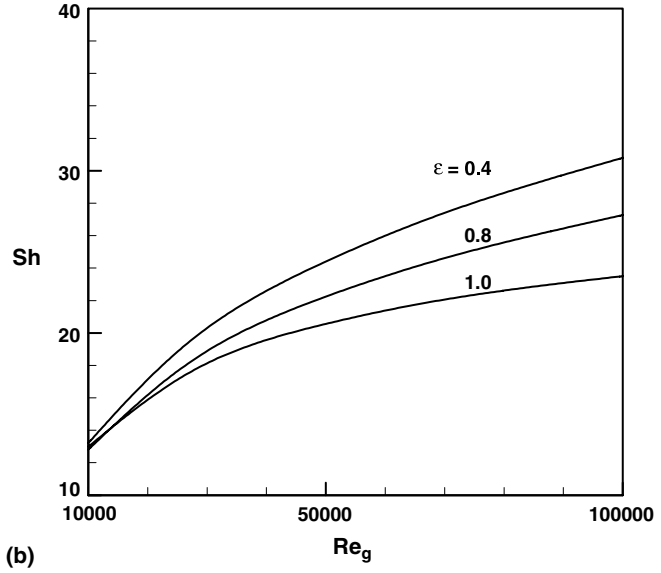

Fig. 6. Variation of the average (a) Nusselt and (b) Sherwood numbers with Re_g for various ε at $\delta = 0.01$ and $\phi = 70\%$.

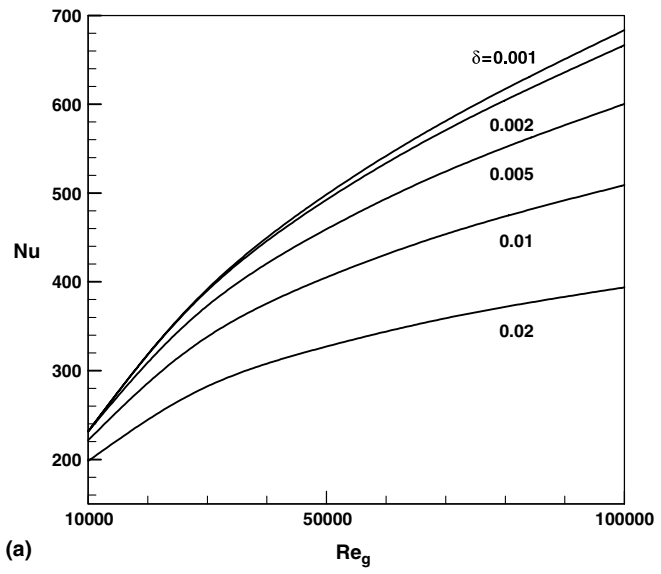

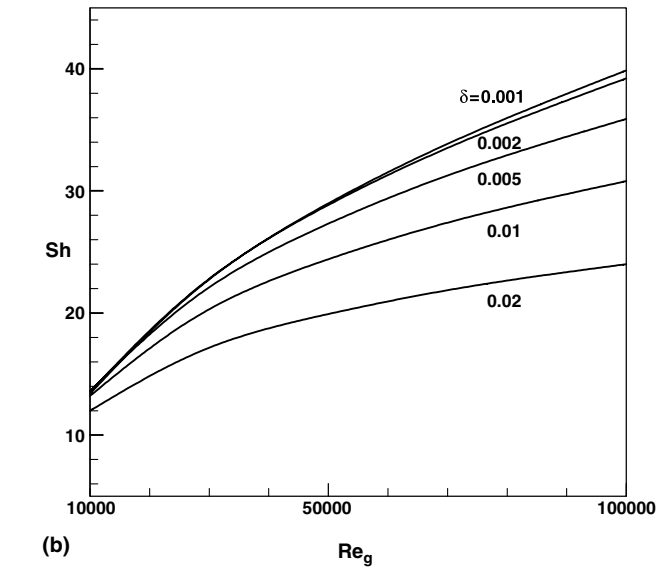

Fig. 7. Variation of the average (a) Nusselt and (b) Sherwood numbers with Re_g for various δ at $\varepsilon = 0.4$ and $\phi = 70\%$.

Fig. 7(a) and (b) illustrate the effect of thickness δ on the heat and mass performance of liquid film evaporation. Calculations were made versus various Re_g for selected porous layer thicknesses ($\delta = 0.001$, 0.002, 0.005, 0.01 and 0.02) at $\varepsilon = 0.4$ and $\phi = 70\%$. It was observed that the larger Nu and Sh are achieved for the cases of thinner δ. This result is because the thicker of porous layer will induce a significant reduction in interfacial temperature and reduce the amount of evaporative vapor. Looking closer it is seen that as $\delta > 0.005$, Nu and Sh are significantly decreased with an increase in δ. Thus, for practical applications, it is recommended that the best operating range for the thickness of the porous layer appears to be within $\delta = 0.001$–0.005. The coupled effects of ε and δ on the Nu and Sh with $Re_g = 50{,}000$ and $\phi = 70\%$ are shown in Fig. 8(a) and (b). It is clearly shown that the Nu and Sh increase as ε is decreased. However, the role of porosity ε is not important for the heat and mass transfer performance when thickness δ is thin ($\delta < 0.005$). The influence of ε on the Nu and Sh is gradually more significant as δ is increased.

The effect of ambient relative humidity ϕ on the Nusselt and Sherwood numbers is illustrated in Fig. 9(a) and (b), respectively. It is found that Nu is higher for lower ϕ. This is because for lower ϕ, Nu possesses higher mass concentration difference between the liquid–gas interface and air stream, resulting in a stronger mass flow rate. However, an opposite trend appears for the Sherwood number, where lower Sh is achieved for lower ϕ. The anomaly results from the larger effect of ϕ on the mass concentration difference ($\omega_w - \omega_\infty$) in Eq. (32) than on the evaporating rate m''_v. From this figure it is also seen that the effect of ϕ on the

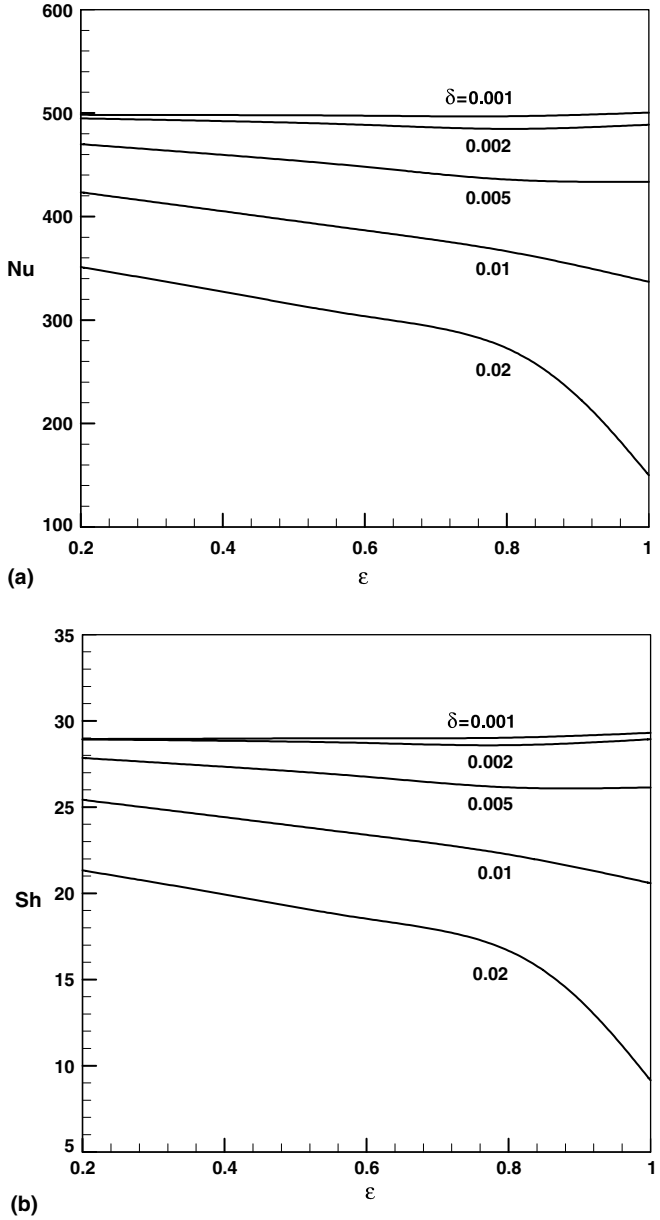

Fig. 8. The coupled effects of porosity ε and thickness δ on the average (a) Nusselt and (b) Sherwood numbers with $Re_g = 50{,}000$ and $\phi = 70\%$.

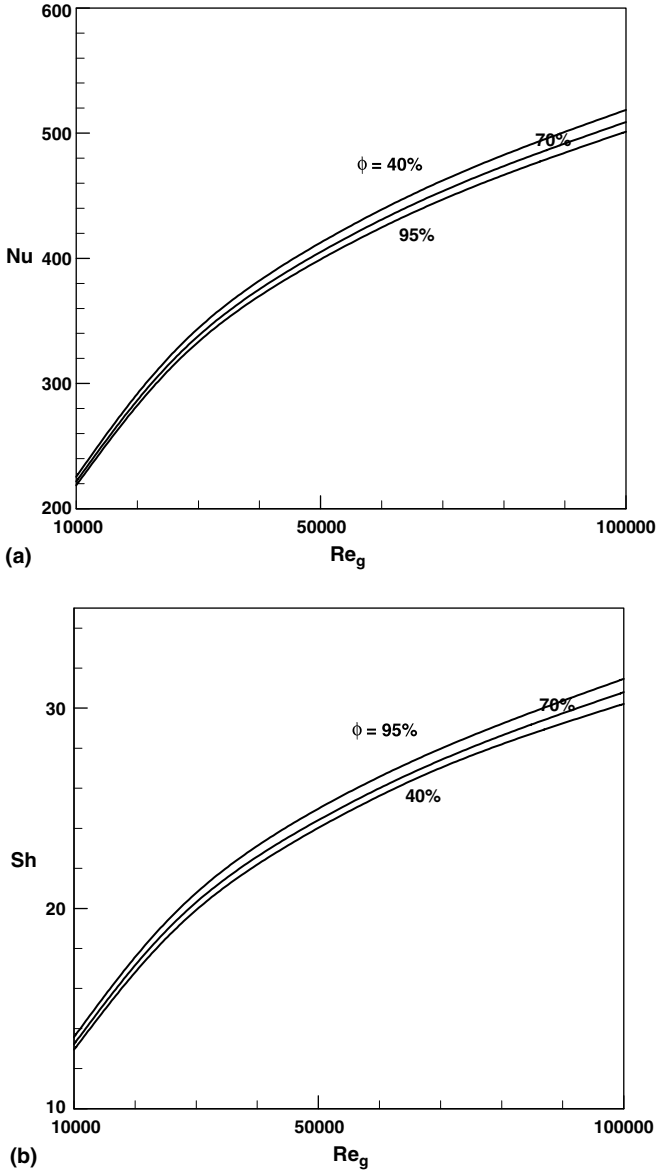

Fig. 9. Variation of the average (a) Nusselt and (b) Sherwood numbers with Re_g for various ϕ at $\varepsilon = 0.4$ and $\delta = 0.01$.

Nu and *Sh* seems to be not significant, when compared with the effects of ε and δ.

To further understand the double diffusion behavior at the liquid–gas interface, the variations of Nusselt and Sherwood numbers versus Re_g for selected Lewis numbers ($Le = 0.1$, 1.0, 10) at $\varepsilon = 0.4$, $\delta = 0.01$ and $\phi = 70\%$ are shown in Fig. 10(a) and (b). The Lewis number ($Le = \alpha/D$) indicates the relative extent of the temperature and concentration fields from the vertical plate. As the Lewis number increases ($Le > 1$), the concentration boundary layer becomes thinner relative to the thermal boundary layer. It is reasonable to expect this leads to a larger mass flow rate and heat transfer rate, and this inference is consistent with Fig. 10, which the *Nu* and *Sh* are higher for larger *Le*.

5. Conclusion

The present investigation provides information about heat and mass enhancement of liquid film evaporation by utilizing the porous layer covered on the plate. The axial distributions of θ_i, λ_i, m''_v, q''_l/q''_t and q''_s/q''_t versus Re_g for selected values of ε, δ and ϕ are numerically described in great detail. In addition, the effects of ε, δ, ϕ and *Le* on the average heat and mass transfer performance are examined. The numerical results conclude that the latent heat flux is the dominant mode for the present study. The cases for lower ε and δ would produce higher interfacial temperature and mass concentration, and thus enhance the heat and mass transfer performances across the film interface. The influence of ε on the *Nu* and *Sh*

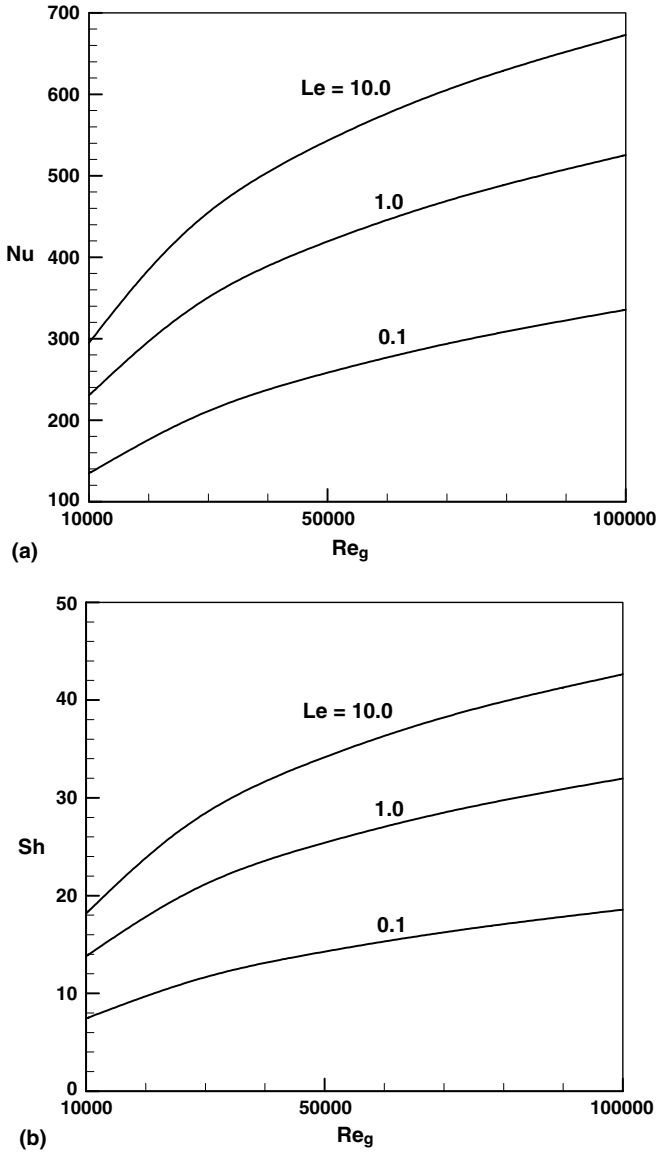

Fig. 10. Variation of the average (a) Nusselt and (b) Sherwood numbers with Re_g for various Lewis numbers with $\varepsilon = 0.4$, $\delta = 0.01$ and $\phi = 70\%$.

is gradually more significant as δ is increased. An applicable range of porous layer thickness $\delta = 0.001$–0.005 is suggested for the practical application. For the effect of ambient relative humidity ϕ, it is observed that a lower ϕ leads to a higher Nu but lower Sh. However, the influence on Nu and Sh appears to be less significant than those of ε and δ. In addition, as the Lewis number increases ($Le > 1$), larger heat transfer rate and mass flow rate are achieved.

Acknowledgement

Financial support for this work was provided by the National Science Council of Taiwan, under contract NSC 93-2622-E-269-003.

References

[1] I.L. Maclaine-Cross, P.J. Banks, Coupled heat and mass transfer in regenerators-prediction using an analogy with heat transfer, J. Heat Mass Transfer 15 (1972) 1225–1242.
[2] I.L. Maclaine-Cross, P.J. Banks, A general theory of wet surface heat exchangers and its application to regenerative evaporative cooling, ASME J. Heat Transfer 103 (1981) 579–585.
[3] A.T. Wassel, A.F. Mills, Design methodology for a counter-current falling film evaporative condenser, ASME J. Heat Transfer 109 (1987) 784–787.
[4] H. Peres-Blanco, W.A. Bird, Study of heat and mass transfer in a vertical-tube evaporative cooler, ASME J. Heat Transfer 106 (1984) 210–215.
[5] B. Gebhart, L. Pera, The nature of vertical natural convection flows resulting from the combined buoyancy effects of thermal and mass diffusion, Int. J. Heat Mass Transfer 14 (1971) 2028–2050.
[6] T.S. Chen, C.F. Yuh, Combined heat and mass transfer in natural convection on inclined surfaces, Numer. Heat Transfer 2 (1979) 233–250.
[7] T.R. Shembharkar, B.R. Pai, Prediction of film cooling with a liquid coolant, Int. J. Heat Mass Transfer 29 (1986) 899–908.
[8] W.W. Baumann, F. Thiele, Heat and mass transfer in evaporating two-component liquid film flow, Int. J. Heat Mass Transfer 33 (1990) 267–273.
[9] W.M. Yan, T.F. Lin, Evaporative cooling of liquid film through interfacial heat and mass transfer in a vertical channel—II. Numerical study, Int. J. Heat Mass Transfer 34 (1991) 1113–1124.
[10] W.M. Yan, C.Y. Soong, Convection heat and mass transfer along an inclined heated plate with film evaporation, Int. J. Heat Mass Transfer 38 (1995) 1261–1269.
[11] Y.L. Tsay, Heat transfer enhancement through liquid film evaporation into countercurrent moist air flow in a vertical plate channel, Heat Mass Transfer 30 (1995) 473–480.
[12] E. Mezaache, M. Daguenet, Effects of inlet conditions on film evaporation along an inclined plate, Solar Energy 78 (2005) 535–542.
[13] J.C. Han, L.R. Glicksman, W.M. Rohsenow, An investigation of heat transfer and friction for rib-roughened surfaces, Int. J. Heat Mass Transfer 21 (1978) 1143–1156.
[14] D.A. Dowson, O. Trass, Mass transfer at rough surfaces, Int. J. Heat Mass Transfer 15 (1972) 1317–1336.
[15] H. Kozlu, B.B. Mikic, A.T. Patera, Turbulent heat transfer augmentation using microscale disturbances inside the viscous sublayer, ASME J. Heat Transfer 114 (1992) 348–353.
[16] G.S. Zheng, W.M. Worek, Method of heat and mass transfer enhancement in film evaporation, Int. J. Heat Mass Transfer 39 (1996) 97–108.
[17] D.A.S. Rees, K. Vafai, Darcy–Brinkman free convection from a heated horizontal surface, Numer. Heat Transfer, Pt A 35 (1999) 191–204.
[18] O.M. Haddad, M.A. Al-Nimr, A.N. Al-Khateeb, Validation of the local thermal equilibrium assumption in natural convection from a vertical plate embedded in porous medium: non-Darcian model, Int. J. Heat Mass Transfer 47 (2004) 2037–2042.
[19] B. Alazmi, K. Vafai, Analysis of fluid and heat transfer interfacial conditions between a porous medium and a fluid layer, Int. J. Heat Mass Transfer 44 (2001) 1735–1749.
[20] T.S. Zhao, Coupled heat and mass transfer of a stagnation point flow in a heated porous bed with liquid film evaporation, Int. J. Heat Mass Transfer 42 (1999) 861–872.
[21] N.A. Diky, N.Y. Koloskova, V.E. Tuz, V.V. Dubrovskaya, Heat and mass transfer and hydrodynamics of liquid evaporation in contact apparatus with a porous packing, Exp. Thermal Fluid Sci. 13 (1996) 85–91.
[22] S. Ergyn, Fluid flow through packed columns, Chem. Eng. Progr. 48 (1952) 89–94.
[23] R.B. Bird, W.E. Stewant, E.N. Lightfoot, Transport Phenomena, John Wiley & Sons, New York, 1960 (Chapter 2).